Supplementary Information (SI) for Physical Chemistry Chemical Physics.
This journal is © the Owner Societies 2024

Supporting Information:

Assignment of IR Spectra of Ethanol at Brønsted Sites of H-ZSM-5 to Monomer Adsorption Using a Fermi Resonance Model

Dipanshu Kumar,[a] Joachim Sauer[b], Alessia Airi, [c,d,*] Silvia Bordiga[d], Daria Ruth Galimberti[*,a]

[a]Institute for Molecules and Materials, Radboud University, Heyendaalseweg 135, 6525 AJ Nijmegen, The Netherlands

[b] Institut für Chemie, Humboldt-Universität, Unter den Linden 6, 10117 Berlin, Germany

[c] INRiM Istituto Nazionale di Ricerca Metrologica, Strada delle cacce 91, I-10135, Turin, Italy

[d] Chemistry Department, University of Turin, via Gioacchino Quarello 15/A, I-10135, Turin, Italy

email: daria.galimberti@ru.nl; a.airi@inrim.it

S1. Structure and morphology of H-ZSM-5 sample

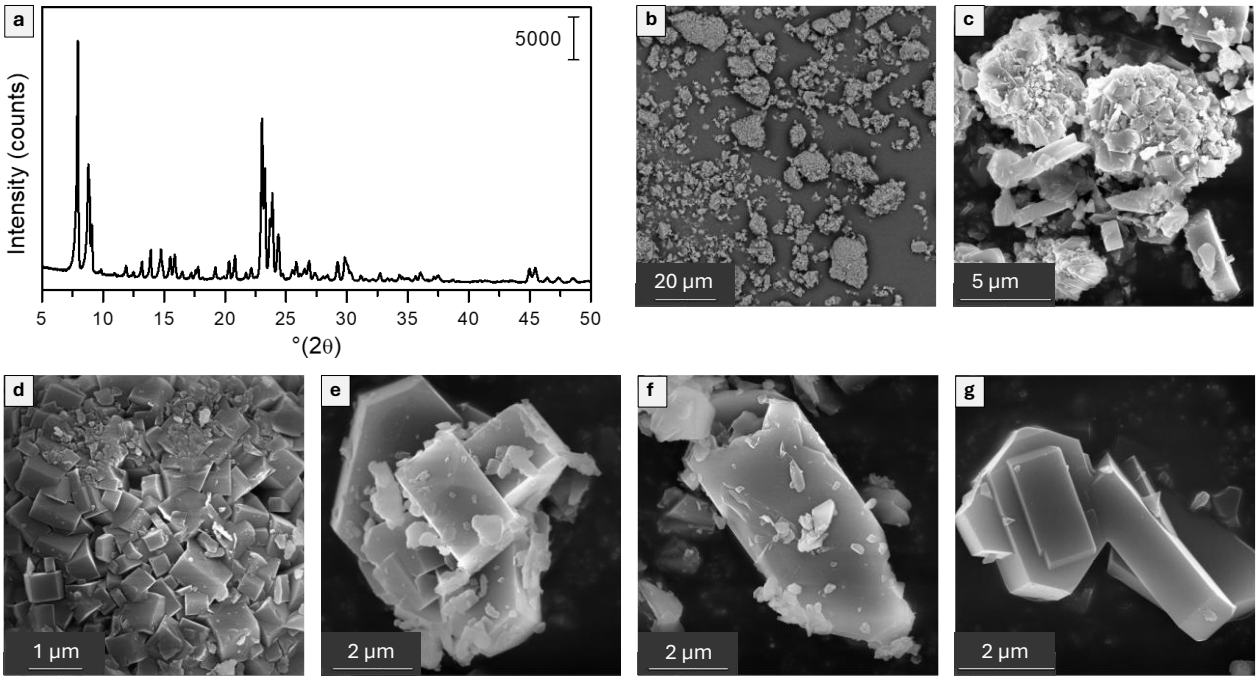

Figure S1. Panel a. Powder X-Ray diffraction of H-ZSM-5 sample in the range 5-50° 2θ angle. Panels b-g. Ultra-high resolution FE-SEM micrographs of H-ZSM-5 sample at different magnifications.

The diffractogram presented in Figure S1a displays the XRD pattern characteristic of the pure MFI framework, as expected. Panels b–g provide UHR FE-SEM micrographs of the powder, revealing its morphology. Panel b shows the presence of large aggregates of crystals, approximately 10–20 µm in size, alongside isolated hexagonal single crystals measuring about 7 µm in length. In panel c, both large single crystals (magnified further in panels e–g) and a cluster of smaller crystals, ranging from 0.5 to 1 µm, can be observed.

The FE-SEM micrographs show that the sample is characterized by unusually large crystals thanks to the prolonged synthesis under carefully controlled conditions. Unlike conventional ZSM-5 materials, typically characterized by nanometric crystals, this sample exhibits crystals on the micrometric scale, often presenting the typical morphology of elongated hexagonal prisms of ZSM-5 crystals (very clear in Figure S1g). The increased crystal size also results in a reduced density of surface defects (both internal and external), as evidenced by the low amount of isolated and h-bonded silanol groups, as discussed in Figure 1 in the main text. Furthermore, the micrometric dimensions of the crystals, combined with their aggregation, account for the pronounced IR radiation scattering visible in the same figure.

S2. Ammonia adsorption on H-ZSM-5 zeolite

The *in situ* ammonia adsorption at room temperature has been followed by FT-IR spectroscopy. Increasing amounts of ammonia has been directly dosed in the home made IR cell over the sample surface, while recording the spectra. The formation of ammonium by protonation of free ammonia by action of Brønsted acidic sites of the zeolite has been monitored by observing the diagnostic modes of the species and the maximum of adsorption is considered when the intensity of the $\nu 4$ fundamental mode (vibrational band at 1450 cm^{-1}) is unchanged by increasing the NH_3 gas amount in the cell. This point is represented by the bold spectrum in Figure S1 and highlighted by vertical line.

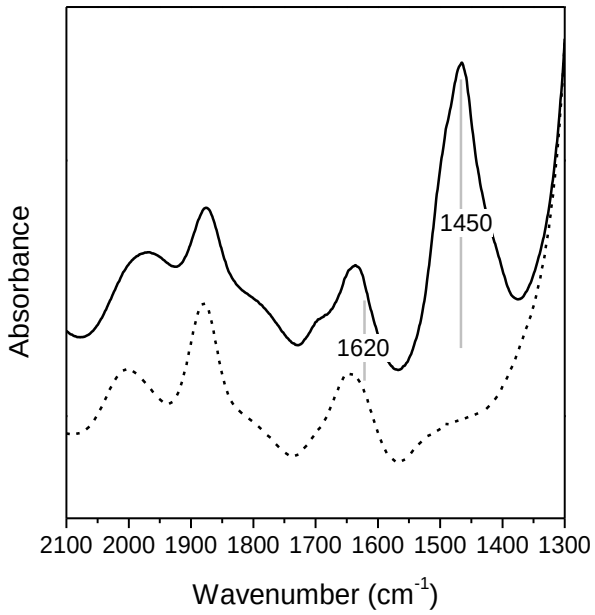

Figure S2. Infrared spectra of activated H-ZSM-5 (dotted line) and in the presence of adsorbed ammonia (bold line) in the diagnostic region of vibrational modes of ammonium (2100-1300 cm^{-1}). The positions of the bands corresponding to δd and ν4 modes of ammonium are indicated by vertical grey lines. The spectra are vertically spaced for the sake of clarity.

The irreversible interaction of free ammonia with the acidic sites of the zeolite forms adsorbed ammonium, which $\nu 4$ fundamental mode[1] generates the vibrational band at 1450 cm^{-1} highlighted in the spectrum of Figure S1. The intensity of this band can be integrated in the Lambert-beer law for calculating the concentration of the corresponding protonic sites, considering the experimental extinction coefficient extracted for the vibrational band in reference.[2] The concentration of Brønsted acidic sites has been calculated with the following equation:

$$BAS\left(\frac{\mu mol}{g}\right) = \frac{A(1450)}{\varepsilon_{BAS}\left(\frac{cm2}{\mu mol}\right)} \cdot \frac{S(cm^2)}{w(g)}$$

Considering $\varepsilon = 0.094\ cm^2\ \mu mol^{-1}$, A is the experimental absorbance extracted from the spectrum of Figure S1, S and w are the area and the weight of the zeolite sample in form of pellet considered as optical path.

The obtained value is around 1700 μmol/g (1.7 mmol/g as reported in the main text) of Brønsted acidic sites, considering an undetermined degree of uncertainty due to the empirical conditions, it is liable to an intrinsic experimental error.

The δ_d mode of ammonium[1] is active when ammonia interacts in tetrahedral configuration electron donor (Lewis base) of uncoordinated metals (Lewis acids), generating a vibrational band at 1620 cm^{-1}. This signal is totally absent in the experimental spectrum reported in Figure S1, as evidenced by the grey vertical line. Therefore, the presence of defects represented by partially uncoordinated or extra-framework aluminum can be reasonably excluded.

S3. Position of the (Z)O–H stretching band for 1 EtOH/BAS

The asymmetric shape of the (Z)O–H stretching band, the non-linear increase of the baseline with the wavenumber, and the contributions of the overtones of framework vibrations make the deconvolution of the (Z)O–H stretching band difficult. A qualitative position for the band can still be deduced from the difference between the incremental variation of the absorbance, dA, just before (0.00600 Torr) and after (0.00675 Torr) reaching the full loading point (green and light blue spectra in Figure 2 of the main text). After the loading is complete, the (Z)O–H stretching band cannot grow further as all possible sites have already been used up; thus, it no longer contributes to $dA^{0.00675}$.
Therefore, we can ascribe the broad asymmetric feature with a maximum around 1670 cm^{-1} in the $dA^{0.00600} - dA^{0.00675}$ spectrum (Figure S2) to the (Z)O–H stretching.
The asymmetry is expected and due to the mechanical coupling of the fundamental "intramolecular" (Z)O–H stretching band with lower frequencies modes, e.g., the intermolecular (Z)OH···O_{Et} stretching vibration and the hindered rotations of the ethanol.

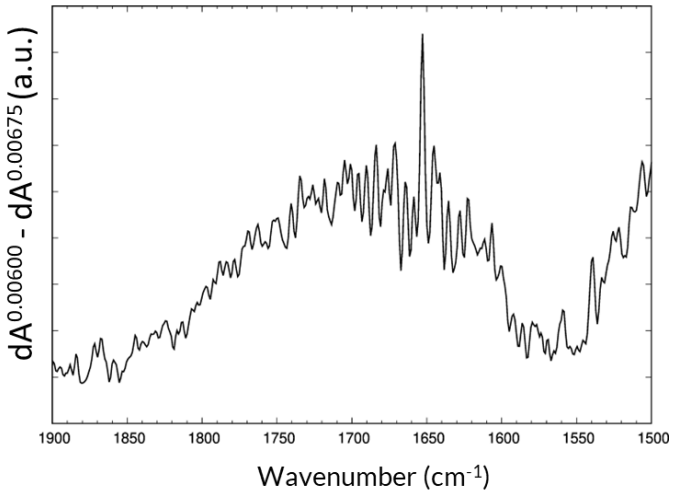

Figure S3. Difference ($dA^{0.00600} - dA^{0.00675}$) between the dA incremental absorbance at 0.00600 Torr and 0.00675 Torr

S4. 1 EtOH/BAS and 2 EtOH/BAS Adsorption geometries

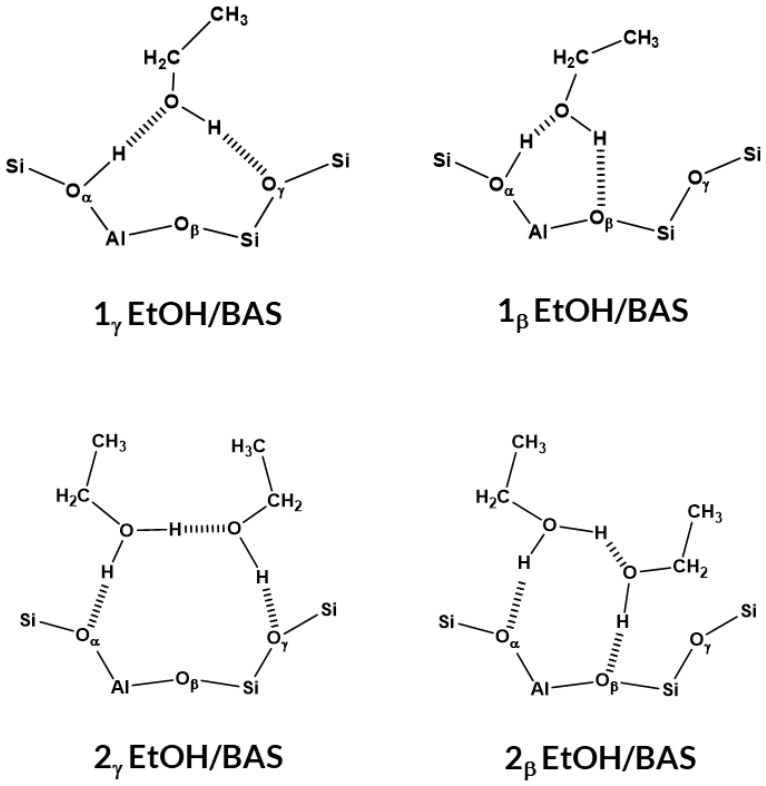

Figure S4. Beta and Gamma arrangements for the monomer ($1_{\beta/\gamma}$ EtOH/BAS) and the dimer adsorption ($2_{\beta/\gamma}$ EtOH/BAS)

We tested two arrangements for the monomer and the dimer adsorption (Figure S3): the first in which the ethanol OH forms an H bond with the framework oxygen atom in gamma position with respect to the aluminum atom (O_γ), and a second in which the ethanol OH forms an H bond with the framework oxygen atom in position beta with respect to the aluminum atom (O_β). Table S1 and S2 show the results obtained for the structures and the differences in electronic energies. In line with what was previously found by Alexopoulos et al.[3], the beta arrangement is either not stable (in the case of 1 EtOH/BAS) or more than 120 kJ/mol higher in energy than the gamma one (in the case of 2 EtOH/BAS). Therefore, it is not relevant at room temperature and, as such, is not discussed in the manuscript. In the main manuscript and the following sections of the Supporting Information, we refer to the gamma arrangement simply with 1 EtOH/BAS and 2 EtOH/BAS.

Table S1. PBE+D2:PBE+D2 and B3LYP+D2:PBE+D2 computed bond distances (pm) for the gamma (1_γ EtOH/BAS) adsorption geometry of 1 EtOH/BAS. The beta (1_β EtOH/BAS) adsorption geometry is not stable.

	PBE+D2:PBE+D2	**B3LYP+D2:PBE+D2**
	1_γ EtOH/BAS	1_γ EtOH/BAS
R1	132.2	140.6
R2	209.7	216.2
(Et)O–H	98.6	97.2
(Z)O–H	113.5	107.2

Table S2. PBE+D2:PBE+D2 and B3LYP+D2:PBE+D2 computed bond distances (pm) for the beta (2_β EtOH/BAS) and gamma (2_γ EtOH/BAS) adsorption geometries of 2 EtOH/BAS. The differences in electronic energies (kJ/mol), $\Delta E_{2\gamma EthOh-2\beta EtOH}$, between the gamma arrangement and the beta one are also reported.

	PBE+D2 :PBE+D2		**B3LYP+D2 :PBE+D2**	
	2_β EtOH/BAS	2_γ EtOH/BAS	2_β EtOH/BAS	2_γ EtOH/BAS
R1	139.7	149.5	141.5	153.2
R3	142.0	139.6	146.8	144.3
R2	185.8	205.3	197.4	209.3
(Et,H)O–H···O_z	106.9	104.9	105.1	103.8
(Et,H)O–H···O(Et,H)	108.2	108.5	104.6	105.4
(Et)O–$H_{\beta/\gamma}$	99.2	98.2	97.4	97.0
$\Delta E_{2\beta EthOH-2\gamma EtOH}$	***140***		***126***	

S.5 Theoretical infrared wavenumber and Infrared absorption intensities

Table S3: PBE+D2:PBE+D2 computed infrared wavenumbers (cm^{-1}) for adsorption on Bronsted Acidic Site (BAS) of H-ZSM-5 of monomer (1 EtOH/BAS) and dimer (2 EtOH/BAS) of ethanol with shifts compared to gas-phase/unloaded H-ZSM-5 (Δ, cm^{-1}) as well as Infrared absorption intensity (I, km/mol) with their respective mode assignments. (ν, stretching; δ, in plane bending; γ, out of plane bending; sym., symmetric; asym., asymmetric)

Scaled[f] (unscaled)		Δ	I	Assignment
Gas/unloaded H-ZSM-5	**1 EtOH/BAS**		**1 EtOH/BAS**	
3616 (3688)	3403 (3471)	-213 (-217)	493	(Et)O–H stretching
3614 (3686)	1386[a] (1414)	-2228 (-2272)	1134	(Z)O–H[b] stretching
2977,2962 (3037,3021) 2936,2883,2841 (2995,2941,2898)	2995,2983 (3055,3043) 2968,2915,2899 (3027,2973,2957)	-32[e] (-33)	19,17 5,29,9	CH_2 and CH_3 stretching
1037 (1058)	1561 (1592)	524 (534)	481	δ(Z–O–H) In-plane Z–O–H bending[c]
273 (278) 162 (165)	1112 (1134)	-895[e] (-912)	289	γ(Z–O–H) Out-of-plane Z–O–H bending[d]
	2 EtOH/BAS		**2 EtOH/BAS**	
3616 (3688)	3461 (3530)	-155 (-158)	313	(Et)O–H stretching
3614 (3686)	-	-	-	(Z)O–H stretching
2977,2962 (3037,3021) 2936,2883,2841 (2995,2941,2898)	3052,3006 2958 2931 (3113,3066,3017,2990) 2986,2983,2975,2919,2906 2892 (3045,3042,3034,2977,2965 2950)	-41[e] (-42)	7,15,8,19 16,7,21,4,14,15	CH_2 and CH_3 stretching
-	2383 (2431)	-	2243	ν_s(O–H)[g] sym
-	1910 (1948)	-	2495	ν_a(O–H)[g] asym
-	1609 (1641)	-	122	δ H–O(Et)–H

a In the low wavenumber range the ZOH and EOH stretching and bending vibrations are heavly coupled by PBE. To recognize the ν(ZOH) (loaded), δ(ZOH) (loaded), γ(ZOH) (loaded), we project the loaded zeolite eigenvectors on the unloaded zeolite ones, and checked the modes with the higher ν(ZOH), δ(ZOH), γ(ZOH) contributions.

b In the case of 1 EtOH/BAS, coupled with the EOH bending, the CH_2 and CH_3 bending

c In the case of 1 EtOH/BAS, coupled with the EOH bending mode and partially with the ZOH stretching

d In the case of 1 EtOH/BAS, coupled with the EOH bending and the CH_2 and CH_3 bending. In the case of the gas-phase EtOH, coupled with the Si-O-Al bending

e average value

f scaling factor: 0.9804

g symmetric and asymmetric stretch for protonated dimer like structure (see main text)

Table S4: B3LYP+D2:PBE+D2 computed infrared wavenumbers(cm^{-1}) for adsorption on Bronsted Acidic Site (BAS) of H-ZSM-5 of monomer (1 EtOH/BAS) and dimer (2 EtOH/BAS) of ethanol with shifts compared to gas-phase/unloaded H-ZSM-5 (Δ, cm^{-1}) as well as Infrared absorption intensity (*I,* km/mol) with their respective mode assignments. (ν, stretching; δ, in plane bending; γ, out of plane bending; sym., symmetric; asym., asymmetric)

Scaled[a] (unscaled)		**Δ**	**I**	**Assignment**
Gas/unloaded H-ZSM-5	**1 EtOH/BAS**		**1 EtOH/BAS**	
3684 (3794)	3531 (3637)	-153 (-157)	406	ν (Et)O–H
3614 (3722)	1806 (1860)	-1810 (-1862)	2958	ν (Z)O–H
2997,2981 (3086,3070) 2962,2905,2883 (3050,2992,2969)	3024,3007 (3114,3097) 2999,2945,2928 (3089,3033,3016)	35[b] (36)	26,23 5,34,10	ν CH_2 and CH_3
1095 (1128)	1530 (1576)	433 (448)	183	δ Z–O–H
372 (383) 217 (223)	1075 (1107)	-	101	γ Z–O–H[c]
	2 EtOH/BAS		**2 EtOH/BAS**	
3684 (3794)	3586 (3694)	-98 (-100)	234	ν (Et)O–H
3614 (3722)	-	-	-	ν (Z)O–H
2997,2981 (3086,3070) 2962,2905,2883 (3050,2992,2969)	3306,3041,2990,2973 (3152,3132,3079,3061) 3018,3015,3000,2957,2947,2921 (3108,3105,3089,3045,3035,3008)	48[b] (49)	9,14,10,19 23,6,25,12,6,14	ν CH_2 and CH_3
-	2565 (2642)	-	2207	sym. ν_s(O–H)
-	2181 (2246)	-	2685	asym. ν_a(O–H)
-	1660 (1710)	-	68	δ H-O(Et)-H

[a] Scaling factor: 0.9710 [b] average value [c] In the case of the gas-phase EtOH, coupled with the Si-O-Al bending [d] symmetric and asymmetric stretch for protonated dimer like structure (see main text)

S.6 Intensity ratio between (f) and (g) features of the experimental spectra

Consider the identified (f) and (g) features of the experimental spectra (Figure 1-B of the main paper) and call $R^{Ex} = \frac{I^f}{I^g}$ the ratio between the integrated experimental absorbance of the region 2700-2000 cm^{-1} (I^f), and between 2000-1500 cm^{-1} (I^g). It is not easy to provide the precise value of R^{Ex} as a function of the pressure due to the already discussed non-linear increase of the baseline with the wavenumber, that makes the removal of the latter not so straightforward. However, it is still possible to quantify $R^{Ex} \gtrsim 0.2$ for pressures between 0.0034 Torr and 0.0060 Torr.

We comment on this lower limit of R^{Ex} in light of the two possible scenarios discussed for assigning the (f) band.

In the following discussion, we use the values computed at the B3LYP+D2:PBE+D2 level.

Let us suppose that the experimental spectrum is the result of a single adsorbed ethanol molecule (1 EtOH/BAS) and that the Fermi resonance model is valid. Then I^f is equal to the intensity of 2γ Z–O–H (2450 cm^{-1}) and the total intensity of I^g is the sum of the contributions of the ν (Et)O–H stretching (1806 cm^{-1}) and the in δ Z–O–H bending (1530 cm^{-1}) vibrations. Therefore

$$R = \frac{I^f}{I^g} = \frac{I_{2\gamma\,\mathrm{Z{\cdot}O{\cdot}H}}}{I_{\nu\ (Et)O{\cdot}H} + I^0_{\delta\ Z{\cdot}O{\cdot}H}}$$

Using eqs S14-S16 and the computed $I^0_{\nu\,(Et)O{\cdot}H}$ and $I^0_{\delta\,Z{\cdot}O{\cdot}H}$, we obtain a theoretical $R^{Th} = 0.36$, compatible with the experimental finding $R^{Ex} \gtrsim 0.2$.

In contrast, let us now suppose that the experimental spectrum is the result of a mixture of a single ethanol molecule (1 EtOH/BAS) and dimer adsorption (2 EtOH/BAS) and that no Fermi resonance is present. We assume that I^f is due to the symmetric OH stretching of the protonated ethanol dimer, ν_s(O–H). This requires the additional assumption that the $\nu_{s/a}$(O–H) stretching of the protonated ethanol dimer are more anharmonic than the other fundamental vibrational bands and that stronger scaling is needed to match the experimental spectrum (see Figure 5 of the main manuscript). If we select for these two bands a scaling factor of 0.9273 (instead of 0.9710), the symmetric stretching, ν_s(O–H), falls at 2450 cm^{-1}, and the antisymmetric one, ν_a(O–H), at 2083 cm^{-1}. However, this is still not enough to reasonably reproduce the experimental spectrum: from our calculations, ν_a(O–H) is around 1.22 times stronger in intensity than ν_s(O–H), but we cannot recognize in the experimental spectrum any band between the 2450 cm^{-1} and 2000 cm^{-1} that can be assigned to ν_a(O–H). Therefore, to proceed with the mixture hypothesis, we need to assume anharmonicity further red-shift ν_a(O–H) band in a way that it is convoluted in the (g) feature. In this case, I^g is the sum of the contributions of the ν_a(O–H) of 2 EtOH/BAS, ν (Et)O–H of 1 EtOH/BAS (1806 cm^{-1}), δ H–O(Et) – H of 2 EtOH/BAS, (1660 cm^{-1}), δ Z–O–H of 1 EtOH/BAS (1530 cm^{-1}).

If we call n the ratio of adsorbed dimers and monomers, the intensity ratio *R* becomes:

$$R = \frac{I^f}{I^g} = \frac{n \cdot I^0_{\nu_s(\mathrm{O{\cdot}H})}}{I^0_{\nu\,(\mathrm{Et})\mathrm{O{\cdot}H}} + I^0_{\delta\,\mathrm{Z{\cdot}O{\cdot}H}} + n \cdot \left(I^0_{\nu_a(\mathrm{O{\cdot}H})} + I^0_{\delta\,\mathrm{H{\cdot}O(Et){\cdot}H}}\right)}$$

Using the computed $I^0_{\nu_s(\mathrm{O{\cdot}H})}$, $I^0_{\delta\,\mathrm{Z{\cdot}O{\cdot}H}}$, $I^0_{\delta\,\mathrm{Z{\cdot}O{\cdot}H}}$, $I^0_{\nu_a(\mathrm{O{\cdot}H})}$, and $I^0_{\nu_a(\mathrm{O{\cdot}H})}$ values, n can be obtained as a function of R. The higher the value of R, the higher the dimers vs. monomers ratio. In particular, when R is equal to 0.2, which is our lower limit, there is one dimer for every three adsorbed single molecules.

S.7 Bandwidth

For an easier comparison with the experimental incremental spectra of Figure 5 in the main text, we assign a Lorentzian shape to the vibrational transitions. A value of 10 cm^{-1} has been chosen for all the spectrum bands except the ones reported in the table below. In consideration of their broad nature in the experimental spectra, larger values have been chosen for them.

	Wavenumbers (cm^{-1}) [a]	**Bandwidth (cm^{-1})**
Unloaded H-ZSM-5	3614 (3722)	20
1 EtOH/BAS	3531 (3637)	50
	2450 (Fermi resonance)	200
	1670 (Fermi resonance)	200
	1530 (1576)	50

[a] Scaled (0.9710), unscaled in parenthesis

S.8 Wavenumber comparison

In Table S5, we report the PBE+D2, B3LYP+D2, ωB97X, and MP2 computed wavenumbers for the ν(Z)O–H stretching, ν(Et)O–H stretching, the δ Z–O–H in-plane bending, and the 2 γ_0 (Z)O–H out of plane bending vibrational modes. The B3LYP+D2 and the ωB97X provide numbers that align with the MP2 ones, with the best match with B3LYP+D2.

The FERMI resonance model requires a certain shift of the fundamental ν_0 ZO-H stretch compared to the 2 γ_0 (Z)O–H and to the experimentally measured $\nu_{\square}$ ZO-H stretch position. MP2 well predicts these. The B3LYP+D2 shift are very close to MP2 – so B3LYP+D2 is sufficient to demonstrate that the FERMI-resonance explains the observed spectra. Instead, PBE+D2 shows substantial deviations compared to the MP2 predictions.

Table S5: ν(Z)O–H, ν(Et)O–H, $\nu_{a/s}$(O–H) stretching and δ Z–O–H, δ H–O(Et)–H bending wavenumbers (cm^{-1}) of 1 EtOH/BAS for different methods. All the computed wavenumbers have been scaled by 0.9710 (B3LYP+D2), 0.9400 (ωB97X), 0.9550 (MP2) and 0.9804 (PBE+D2). In parenthesis, the shift compared to the gas phase ethanol/the unloaded H-ZSM-5.
sym.=symmetric; asym.=asymmetric; v=stretching; δ=in plane bending; γ=out of plane bending;

	PBE+D2	**B3LYP+D2**	**ωB97X**	**MP2**
ν (Et)O–H	3403 (-217)	3531 (-157)	3528(-118)	3496 (-147)
ν_0 (Z)O–H	1386 (-2228)	1806 (-1808)	2257(-1357)	1897(-1717)
2 γ_0 (Z)O–H	2224	2150	1895	2086
δ Z–O–H	1561 (534)	1530 (433)	1392 (352)	1450 (395)

Bibliography

1. Suganuma, S.; Murakami, Y.; Ohyama, J.; Torikai, T.; Okumura, K.; Katada, N., Assignments of Bending Vibrations of Ammonia Adsorbed on Surfaces of Metal Oxides. *Catal. Letters* **2015,** *145*, 1904-1912, https://doi.org/10.1007/s10562-015-1592-6.
2. Weglarski, J.; Datka, J.; He, H.; Klinowski, J., IR spectroscopic studies of the acidic properties of the mesoporous molecular sieve MCM-41. *J. Chem. Soc., Faraday Trans.* **1996,** *92*, 5161-5164, https://doi.org/10.1039/FT9969205161.
3. Alexopoulos, K.; Lee, M.-S.; Liu, Y.; Zhi, Y.; Liu, Y.; Reyniers, M.-F.; Marin, G. B.; Glezakou, V.-A.; Rousseau, R.; Lercher, J. A., Anharmonicity and Confinement in Zeolites: Structure, Spectroscopy, and Adsorption Free Energy of Ethanol in H-ZSM-5. *J. Phys. Chem. C* **2016,** *120*, 7172-7182, https://doi.org/10.1021/acs.jpcc.6b00923.